Author version: *J. Indian Assoc. Sedimentol., vol.31(1&2); 2012; 123-135.*

Coarse fraction components in a red-clay sediment core, Central Indian Ocean Basin: their occurrence and significance

Sridhar D. Iyer[1], Glancia Q. Fernandes[1,2] and K. Mahender[2]

[1]National Institute of Oceanography (CSIR), Dona Paula Goa 403 004, India. iyer@nio.org, Phone: 0832-2450263, Fax: 0832-2450602

[1,2]Department of earth Science, Goa University, Bambolim, Goa 403 206, India. queenieglanica@gmail.com

[2]Department of Earth Science, Goa University, Bambolim, Goa 403 206, India. mkotha@yahoo.com

Abstract

We report coarse fractions components of a sediment core (268 cm from a water depth of 5120 m) collected at 18^{o} S and 80^{o} E from the red clay domain in the Central Indian Ocean Basin (CIOB). The components are mineral grains, basaltic fragments, phillipsite, ferromanganese micronodules, glass shards, small pumices, microtektites and biogenic material. This paper describes the provenance of these coarse fraction components that have resulted from multiple sources - both in situ and derived products.

Key Words: Sediment core, coarse fraction, genesis, CIOB

Introduction

Marine sediments show distinct variations in terms of their colour, texture, component and composition and derived from erosion of the continents, from organisms (shell and organic matter), seawater precipitation (salts), volcanism (ash, pumice) and also from extraterrestrial source (cosmic spherules, dust, tektites) (cf. Lisitzin, 1996). Of these sources the most significant is weathering of terrestrial rocks while “weathering” at the ridge crests and other young marine volcanic features result in hydrothermal or metalliferous sediments.

There have been several studies on the sediment distribution and processes responsible in the Central Indian Ocean Basin (CIOB), a basin which receives sediments from two of the large rivers in the world i.e., Ganges and Brahmaputra (Nath et al., 1989) and also holds potential ferromanganese (FeMn) nodule deposits in the world oceans. The nature and distribution of sediments in the Indian Ocean are principally controlled by interrelated factors (cf. Mukhopadhyay et al., 2008): climatic and current patterns, nutrient and organic production in surface waters, relative solubility of calcite and silica, and submarine topography and detrital input. The major types of sediments in the CIOB are terrigenous, calcareous, siliceous and pelagic.

We investigated a sediment core of 268 cm long collected from a water depth of about 5120 m from the CIOB (latitude 18° S and longitude 80° E) in red clay domain where studies are sparse. The paper describes coarse fraction components – their shape, size, texture and chemical composition and discusses their source of derivation.

MATERIALS AND METHODS

Several workers have investigated cores from different sediment domains of the CIOB (Nath et al., 1992; Nath, 2001 and references therein). A majority of these cores studied are from the siliceous ooze and were examined mainly from geochemical point of view and occurrence of micronodules and microtektites (cf. Mukhopadhyay et al., 2008).

Bulk sampling for FeMn nodules and deep-tow operations were carried out during the 7th cruise onboard the Russian chartered vessel AA Sidorenko. During the cruise three gravity cores were collected, 16°S, 17°S and 18°S along 80°E. A gravity core (GC-1) was collected which was 268 cm long from a water depth of 5120 m at latitude 18° S and longitude 80° E. The core was sub-sampled at 2 cm interval on-board and the colour variations were noted by comparing with the Munsell rock colour chart. All the samples were oven dried at 60-70 °C and were wet sieved (+63 µm). The coarse fractions were dried, weighed and stored in vials.

An OLYMPUS SZX7 binocular microscope was used to study the particles (Table 1) at magnifications between X8 and X56. Photomicrographs at different magnifications were obtained using an OLYMPUS SZX16 attached with a digital camera. The particles from different sub-sections of the core were mounted on stubs fixed with a carbon tape and a scanning electron microscopy (SEM, JEOL JSM-5800LV) was used to examine the particles (magnifications from X120 to X850) and the composition of the particles was determined with an energy dispersive spectrometre (EDS, OXFORD LINK).

GEOLOGY OF THE CIOB

The CIOB with an area of ~5.6 x10^6 sq km (average water depth is ~5000 m) has ore grade FeMn nodule deposits (Sudhakar, 1989). The basin is bordered to the north and southeast by plate boundaries between India and Australia and Australia and Capricorn, respectively and to the west and east by the aseismic ridges such as the Chagos-Laccadive Ridge and the Ninetyeast Ridge, respectively. The CIOB, generated from the Indian Ocean ridge system during the Paleocene (Royer et al., 1989) is characterised by several ridge-normal lineaments and fracture zones (FZ) which considerably influenced the volcanic and tectonic environment in terms of formation and distribution of seamounts, abyssal hills and FeMn deposits. The important FZ are Vishnu along 73° E and Indrani along 79° E and the Triple Junction Trace on the Indian plate located along longitude 76° 30’ E (Dyment, 1993; Das et al., 2007).

The CIOB hosts several seamounts, of variable dimensions, in the form of linear chains or as isolated entities. Most of the seamounts are flat topped while some have craters and the mean flatness decreases with increasing height (Das et al., 2007). During the reorganisation of the tectonic plates the Central Indian Ridge and South East Indian Ridge moved to the present sites and in the process resulted in propagative fractures and subsequent volcanism produced the seamounts (Das et al., 2007).

The four major sediment types in the CIOB are terrigenous, calcareous, siliceous and red clay. Terrigenous sediments, cover ~14% of the basin, have the highest rate of sedimentation, are largely detrital and are transported by Ganges and Brahmaputra up to 8^{o} S (Nath et al., 1989; Lisitzin, 1996). About 35% of the basin is covered by calcareous sediments (sedimentation rate 4-6 mm/10^3 year) that commonly occur along the equatorial high productivity areas and at shallower water depths, such as near the Chagos and Ninetyeast Ridges and the shallow areas of seamounts (west of 74^{o} E). Siliceous (extends from 8^{o} to 15^{o} S) and red clay (south of 15^{o} 30' S) are the dominant sediment types in the southern regions of the basin and cover about 35 and 16%, respectively. These sediments occur due to low rate of sedimentation (< 2 mm/10^3 year) and terrigenous contribution is minimal or absent. The eupelagic red clay contains <25% lithogenous or volcanic components (Mukhopadhyay et al., 2008).

The volcanics in the CIOB are tholeiitic basalts, ferrobasalts, spilites and pumice. In addition, glass shards, palagonite, zeolitic slabs of phillipsite and volcanogenic-hydrothermal material also occur in the sediments. The seafloor basalts of the CIOB have been subjected to different degrees of alteration and this has produced palagonite from basaltic glass, sericite from plagioclase and iddingsite from olivine (Iyer, 1999).

Several tephra beds, pumice clasts and dispersed rhyolitic glass shards occur in the Pliocene and Quaternary sediments of the CIOB (Martin-Barajas and Lallier-Verges, 1993; Iyer and Sudhakar, 1995; Iyer et al., 1997). For instance, the super-eruption of Toba volcano in northern Sumatra about 74 ka ago (Rose and Chesner, 1987) resulted in widespread fallout of tephra to more than 3000 km in a northwesterly direction (Ninkovich et al., 1978; Dehn et al., 1991). On the contrary, Sukumaran et al. (1999) suggested that the shards are the products of sub-oceanic volcanism during the onset of glaciations. Iyer et al. (1997) and Mascarenhas-Pereira et al. (2006) attributed intrabasinal as a source of these materials.

Zeolites are important diagenetic minerals in deep sea sediments and of these, phillipsite and clinoptilolite are most common. Phillipsite is more abundant in the Pacific and Indian oceans than in the Atlantic (Kolla and Biscaye, 1973; Kastner and Stonecipher, 1978) and occurs mainly in Miocene sediments and younger. In the Indian Ocean, natrolite, phillipsite, clinoptilolite and nontronite also occur (Kastner and Stonecipher, 1978; Iyer et al., 1997; Mascarenhas-Pereira and Nath, 2010). Diagenetically, well-formed phillipsite crystals form within manganese micronodules of the CIOB (Banerjee and Iyer, 1991). Consolidated slabs of zeolites occurring in the CIOB form nuclei and substrate for the deposition of FeMn oxides (Iyer and Sudhakar, 1993b; Iyer et al., 2007).

From the above information it is obvious that the CIOB has a variety of morpho-tectonics features (FZ, seamounts) and several types of volcanics (basic to silicic). The source of the volcanics is largely in situ (intraplate volcanism) and some derived products from land volcanoes. The sediments contain glass shards, altered rock pieces, zeolites, FeMn micronodules and tektites. The major biota is dominantly radiolarians along with diatoms, ichthyoliths (fish teeth), sharks' teeth and phytoliths (plant remains). Moreover, there are evidences that the basin witnessed localised hydrothermal activity that resulted in the formation of ochrous sediments and spherules of magnetite, titanium and aluminium (Iyer, 2005; Iyer et al., 2007b). All these suggest that the CIOB is a dynamic basin and suggests the possibility of tectonic or volcanic activity in the present day.

RESULTS AND DISCUSSION

The weight and percentage of coarse fraction up to 100 cm at an interval of 2 cm of the studied core GC-1 are provided (Table 1, Fig. 1). The coarse fraction is generally less than 1% except between 0 and 2 cm, 2 and 4 cm and 4 and 6 cm depth intervals where it is 1.86%, 1.41% and 1.15%, respectively due to the abundance of glass shards (Fig. 1) while the peaks at 68-70, 76-84, 96-98 cm is due to the presence of micronodules. The components (Table 2) were examined for abundance, shape, size, colour and surface features.

In core GC-1 a maximum of 206 number of micronodules occur between 56 and 58 cm core depth followed by 171 number between 68 and 70 cm. Glass shards are of two types: transparent and translucent. A preliminary observation of the scarp samples (i.e., the sediments stuck to the core liner) shows an abundance of translucent shards with depth especially between 100 and 150 cm and this form 60-65% of the total shard population. The colourless glass shards are of three morphotypes: (i) blocky with shapes ranging from spherical to oval, (ii) platy and (iii) bubble walled or Y-shaped.

Phillipsite occurs as prismatic, colourless to yellowish grains and form twinned crystals that show 2 or more intersecting twin planes. The crystals are either fresh and while a few show features of dissolution in the form of pores or pits. The pumices have ellipsoidal, elongated and spherical vesicles and also form nuclei for FeMn oxides. The basaltic fragments are fresh with thin glass veneer or show iron oxide stains.

The minor minerals are biotite and quartz. Biotite grains are black, flaky, show a sub-vitreous luster and very distinct basal cleavages. Quartz grains are transparent, rounded to sub-rounded and have conchoidal fractures. Besides these, there are also microtektites and broken fragments of microtektites with impact features on their surface and several volcanic magnetite spherules. The biogenic matter includes fish teeth (whole and fragments), phytoliths and radiolarians. The radiolarians are nearly absent below 18 cm.

SEM-EDS studies: Biotite grains are fresh in appearance, have sharp edges, depict perfect sets of basal cleavage and are 145 µm to 470 µm long (Fig. 2). Phillipsite grains of 143 µm to 309 µm length occur as single or multiple intersecting crystals with or without a veneer of FeMn oxides (Figs. 3, 4). A spherical microtektite (309 µm) shows numerous impact features (Fig. 4D).

The radiolarians have variable morphology and range between 141 µm and 246 µm and the skeletons have sharp and dense spicules (Fig. 5 A-C). The fish teeth are flat to nearly conical and are 185 µm to 733 µm long (Fig. 5 D-F). FeMn micronodules are spheroidal to sub-spheriodal, elongated and also polynucleated and vary from 206 µm to 745 µm (Fig. 6) and some of the micronodules host crystals of phillipsite (Fig. 6B).

Glass shards are either transparent (Fig. 7 A,B) or translucent (Fig. 7 C,D). The former are 227 to 411 µm long and are either platy or bubble or Y-shaped morphology while the translucent shards are 46 to 190 µm long and are blocky or flat and stubby (Fig. 7 E,F). Coloured glass is also present of spherical to sub-spherical shapes while some grains are irregular or blocky. Iron-rich fragments are nearly triangular or blocky and are 224 to 735 µm long (Fig. 8 A,B). Pumices of different shapes are 183 to 850 µm in size (Fig. 8 C-F) and sometimes have FeMn oxides and phillipsite crystals (Fig. 8 F). The above components were analysed and the average composition is shown in table 3.

Down-core compositional variations of selected components (phillipsite, FeMn micronodules, glass shards and pumice) were observed. The SiO_2% in phillipsite decreases and then increases continuously upto 20-22 cm with 70.33% and this indicates that the phillipsite crystals have undergone dissolution at 8-10 cm depth. This is seen as dissolution pits on crystals (Fig. 4 A-C). Al_2O_3 and CaO contents decrease and increase at 36-38 cm with a change of 4.91% and 11.2%, respectively. TiO_2 FeO, MgO, Na_2O, K_2O show an almost uniform trend with depth. MgO follows a trend as that of MnO while FeO shows an almost uniform trend. The inverse relation between MnO, MgO and with SiO_2 could be due to diagenesis. The enrichment of MnO and MgO in the micronodules leads to a partial depletion in SiO_2. SiO_2 has a peak of 27.71% at 56-58 cm and MnO a peak of 54.6% at 72-74 cm.

In the glass shards, SiO_2 decreases from 80% to 40% at 56-58 cm and then increases to about 80% at 62-64 cm. At a depth of 56-58 cm CaO and FeO show a peak of 22.76% and 14.21%, respectively. At 56-58 cm SiO_2 decreases to about 40% and CaO and FeO increase indicating that SiO_2 has an inverse relation to CaO and FeO. These observations suggest that perhaps there are two generations of shards: one at <2 cm and 68-70 cm and the other between 56 and 58 cm. Al_2O_3 ranges between 10 and 20 while TiO_2, MgO, Na_2O, K_2O show a nearly uniform trend. Pumices show a very uniform trend in SiO_2, Al_2O_3, TiO_2, FeO, MgO, CaO, Na_2O, K_2O, NiO and MnO with depth suggesting their origin from a single volcanic episode or from similar magma type.

Summing up the detailed microscopy observations it is noted that micronodules peaks between 56 and 58 cm while shards decrease with depth and have a variable morphology. Phillipsite varies with depth and shows multiple twins, overgrowths and dissolution pits. Pumices have variable morphology, host phillipsite and may have FeMn oxide coating. The other components are rock fragments, mineral fragments (mainly biotite, quartz) and biogenic matter (radiolarians and fish teeth). Microtektites and Fe-rich fragments are sparse.

The composition of the components corresponds with that reported by Deer et al. (1967) for biotite flakes, the micronodules are similar to those of Banerjee and Iyer (1991), phillipsite crystals correspond to those of Iyer at al. (2007b), the pumice clasts resemble that reported by Iyer and Sudhakar (1993b), the microtektite is similar to that reported by Prasad (1994) while the Fe-rich fragments resemble magnetite spherules (Iyer et al., 1997).

DISCUSSION

Based on the results and observations we discuss the probable source and origin of the micronodules, glass shards, phillipsite crystals, pumice clasts, rock fragments, mineral grains (biotite, quartz) and biogenic matter present in the core GC-1 (Tables 2,3). The biotite and quartz grains are derived from the altered granitic rocks of the Himalaya and transported by the rivers Ganges and Brahmaputra. This observation is also attested by the study of Nath et al. (1989) who reported the occurrence of terrigenous material up to 10^o S. Biotite being flaky and quartz being a resistant mineral could have withstood such long distance transport and finally settled at the present core site. This observation suggests that perhaps the influence of terrigenous input extends at least up to 18^o S latitude in the CIOB.

Marine authigenic phases, such as phosphorites, manganese nodules, feldspar grains, metal-rich sediments and zeolites, play a role in the geochemical cycling of elements in – seawater and sediments. Zeolites constitute up to 80% of oceanic and volcaniclastic sediments and their composition depends, among other factors on the following: reaction time for devitrification,

crystallochemical transformations of glass of different Si/Al ratios at low, temperature and pressure, sedimentation rates, sediment type, and Eh-ph conditions (Iyer et al., 2007a).

Authigenic minerals form by: hydrogenous, diagenesis, hydrothermal, metamorphism and halmyrolysis processes. The two possible precursors for the formation of zeolites in the CIOB are a continuous layer of volcanic ash and / or altered fragments of pumice and devitrification of basaltic glass (Iyer and Sudhakar, 1993a). Phillipsite in oceanic sediments occurs as single or as multiple twinned crystals. Crystals of twinned phillipsite are present at various depth intervals in core GC-1 and display two or more twin planes (Figs. 3, 4) that form interpenetrative crystals and are unlike the single crystals reported by Banerjee and Iyer (1991). According to Kastner and Stonecipher (1978) the nucleation and growth of phillipsite occur at the sediment/water interface and the crystal could continue to grow within the sediment column. Phillipsite also undergoes rapid dissolution and results in etched crystal faces or complete disappearance of the crystal form. The processes of rapid growth and dissolution indicate that phillipsite formation is kinetically controlled. Phillipsite coexists with smectite, Fe-oxyhydroxides and FeMn oxides and almost always with basaltic glass (Kastner and Stonecipher, 1978). It has been shown that the reaction involving basaltic glass and dissolved silica (primarily biogenic) could also form phillipsite (Czyscinski, 1973). Therefore, the presence of rock fragments (basaltic, pumiceous) in the core GC-1 suggests the formation of phillipsite from these precursors.

Ferromanganese micronodules form in areas of low sedimentation (Ericson and Wollin, 1973). In the core GC-1, micronodules are spherical and irregular in shapes, have rough and botryoidal textures and 206 μm to 745 μm in size (Table 2; Fig. 6). Between 56 and 58 cm core depth, 206 micronodules occur followed by 171 counts at 68-70 cm core depth. Mukhopadhyay et al. (1988) have reported that the abundance of micronodules from the siliceous and red clay sediments of the CIOB is related to the effects of early diagenesis and micronodules do not enhance the growth of associated macronodules present at the sediment-water interface. Banerjee and Iyer (1991) noted a link between the dissolution of siliceous biota and formation of micronodules.

Glass shards are ubiquitous in the sediments of the CIOB and tend to be dominant in the siliceous sediment. In the core GC-1 transparent (Fig. 7 A,B) and translucent (Fig. 7 C,D) shards occur at different depths. The CIOB shards have three different morphologies (Mascarenhas-Pereira et al., 2006): blocky with a few vesicles, the shape of which range from spherical to oval and produced by hydroclastic processes; platy, which are formed from the glass walls separating large flattened vesicles and, bubble walled or Y-shaped, which represent the remnants of three bubble junctions, or double concave plates that formed the wall between adjoining bubbles (Fisher and Schmincke, 1984). In core GC-1, the shards are mostly platy and /or exhibit Y-shaped morphology. The colourless shards are rhyolitic while those with TiO_2 are red, orange or green in colour.

The shape of individual fragmented clast is usually related to its mode of interaction with water (Wohletz, 1983). This is attested by the shards that have irregular and angular fractures that resulted due to rapid quench and fragmentation during the interaction between magma and water. The shape of the shards is affected by many variables, particularly pumice shards tend to develop from relatively high viscosity rhyolitic magma at a temperature <850 ^{o}C, whereas bubble wall shards tend to develop from lower viscosity rhyolitic magma at a temperature >850 ^{o}C (Izett, 1981).

The source of the shards in the Indian Ocean is reported to extend to the east and south of the Indonesian Volcanic Arc (IVA) and up to Antarctica (Rose and Chesner, 1990) and in the north into the Bay of Bengal (Rose and Chesner, 1987). These shards are the products of the supereruption of the Toba volcano (about 74 ka ago) located in the IVA. Some of the CIOB shards correspond to that of Toba but interestingly, an in situ origin for the glass shards have also been forwarded (Iyer et al., 1997; Sukumaran et al., 1999; Mascarenhas-Pereira et al., 2006). Thus, it appears that the shards might have a mixed origin i.e., from the Toba and also from deep water volcanic eruptions. Interestingly, as pumice is transported across the ocean it could be worn down and the resulting fine material, similar to ash, is scattered on the ocean floor. Therefore, it would be pertinent to note that all the reported shards need not necessarily belong to the IVA but may also have been derived from breakdown of pumice clasts. Such a process would lead to erroneous estimates and distribution of shards in the CIOB sediments.

The particles of palagonite, formed from the alteration of the basalts, are porous, have variable colours (orange, straw yellow, pale brown) and a waxy lustre. Rock fragments (resembling baked sediments) present in the core GC-1 are either fresh or altered (Table 1; Fig. 8 A,B) and might have been derived through volcanic or hydrothermal activities. The microtektites (Table 1, Fig. 4 D) suggest these to belong to the Australian microtektite strewn field in the CIOB (Prasad, 1994).

Alteration and induration of pumice could form zeolitic slabs since in some samples pumice occur entrapped within the slabs, an observation that indicates a siliceous precursor for the CIOB zeolites (Iyer and Sudhakar, 1993b). Mafic precursors are more common and under favourable conditions these are transformed into zeolites through a stage of palagonite formation (Iyer, 1999). A similar association of phillipsite and palagonite / smectite, in the Pacific Ocean was attributed to the reaction of interstitial water with sedimentary particles (especially shards) at low temperature during diagenesis (Honnorez, 1981). The studied core consists of phillipsite crystals as well as small pumices that attest to the above observations.

The CIOB pumices are buff, grey, black and brown in colour and oval, lineated, sub-rounded, rounded and irregular in shape (Iyer and Sudhakar, 1993b). Small pieces of rhyolitic pumice commonly occur at various depth intervals in the core GC-1 (Table 2; Fig. 8). The CIOB pumices have been ascribed to the following sources: transportation from the 1883 eruption of Krakatoa volcano (Indonesia) (Iyer and Karisiddaiah, 1988; Martin-Barajas and Lallier-Verges, 1993) and in situ eruption on the seafloor (Svalnov, 1981; Iyer and Sudhakar, 1993b) or combination of 1 and 2 (Mukherjee and Iyer, 1999).

SUMMARY AND CONCLUSION

An examination of a gravity sediment core recovered from the CIOB reveals several components such as mineral and rock fragments, phillipsite grains, ferromanganese micronodules, glass shards, Fe-rich fragments, microtektites, and biogenic matter (radiolarians, phytoliths and fish teeth). These components have been derived from different sources. For instance, (1) biotite and quartz grains are brought from the altered granites of the Himalaya through Ganges and Brahmaputra rivers, (2) diagenesis and halmyrolysis of the basaltic glass form phillipsite, (3) micronodules form through diagenesis, (4) glass shards have a mixed origin i.e., from the ~74 ka eruption of Toba volcano and also from abyssal volcanic eruptions, (5) rock fragments are the products of volcanic events, (6) pumices were perhaps transported from the 1883 eruption of

Krakatoa and/or are from in situ intraplate eruptions. Detailed investigations of the chemistry of the sediment core could help understand the formational history of the coarse fraction components.

ACKNOWLEDGEMENTS: We thank the Director NIO, for extending facilities to GQF to carry out this work as a part of her MSc dissertation. Dr. M. Shyam Prasad and V.M. Khedekar assisted with binocular microscopy and SEM-EDS, respectively. Ms. Ruenna D'Souza provided secretarial help. We acknowledge the comments of the reviewer that helped to vastly improve the presentation and the encouragement by Prof. D.R. Reddy (Editor) to carry out the revision. This is NIO's contribution **#???.**

REFERENCES

Banerjee, R. and Iyer, S.D., 1991. Biogenic influence on the growth of ferromanganese micronodules in the Central Indian Basin. *Mar. Geol*., **97,** 413-421.

Czyscinski, K., 1973. Authigenic phillipsite formation rates in the Central Indian Ocean. *Deep-Sea Res*., **20,** 555-559.

Das, P., Iyer, S.D. and Kodagali, V.N., 2007. Morphological characteristics and emplacement mechanism of the seamounts in the Central Indian Ocean Basin. *Tectonophys.*, **443**, 1-18.

Deer, W.A., Howie, R.A. and Zussman, J., 1967. An introduction to the rock forming minerals. Longmans, London, UK, 270 pp.

Dehn, J., Farrel, J.W. and Schmincke, H.-U., 1991. Neogene tephprochronology from site 758 of the northern Ninetyeast ridge: Indonesia arc volcanic of the past 5 Ma. In: Proceedings of the Ocean Drilling Projects, Scientific Results (J. Peirce, J. Weissel and E. Taylor, eds.), **121**, pp.273-295. College Station, TX.

Dyment, J., 1993. Evolution of the Indian Ocean Triple junction between 65 and 49 Ma (anomalies 28 to 21). *Jour. Geophys. Res.,* **98,** 13863-13878.

Ericson, D.B. and Wollin, G., 1973. Precipitation of manganese oxide in deep-sea sediments. In: *Inter-Univ. Program Research in Ferromanganese Deposits of the Ocean Floor. Phase I Report* (R.D. Gerard, ed), Nat. Sci. Found, Washington, D.C., pp. 99-103.

Fisher, R. V. and Schmincke, H. -U., 1984. Pyroclastic rocks. Springer, Berlin, 472 pp.

Honnorez, J., 1981. The aging of the oceanic crust. In: The Sea (C. Emilian, ed.), **7**, pp.525-587. John Wiley and Sons, New York.

Iyer, S.D., 1999. Alteration of basaltic glass from the Central Indian Ocean. *Jour. Geol. Soc. India,* **54,** 609-620.

Iyer, S.D., 2005. Evidences for incipient hydrothermal event(s) in the Central Indian Basin: A Review. *Acta Geologica Sinica*, **79,** 77-86.

Iyer, S. D. and Karisiddaiah, S. M., 1988. Morphology and petrography of pumice from the Central Indian Ocean Basin. *Indian Jour. Mar. Sci*., **17**, 333-334.

Iyer, S.D. and Sudhakar, M., 1993a. A new report on the occurrence of zeolitites in the abyssal depths of the Central Indian Basin. *Sed. Geol*., **84,** 169-178.

Iyer, S.D. and Sudhakar, M., 1993b. Coexistence of pumice and manganese nodule fields-evidence for submarine silicic volcanism in the Central Indian Basin. *Deep-Sea Res.,* **40,** 1123-1129.

Iyer, S.D. and Sudhakar, M., 1995. Evidences for a volcanic province in the Central Indian Basin. *Jour. Geol. Soc. India*, **46**, 353-358.

Iyer, S.D., Sudhakar, M. and Das, P. 2007a. Composition and genesis of zeolitic claystones from the Central Indian Ocean Basin. *Acta Geologica Sinica*, 81: 756-770.

Iyer, S.D., Mascarenhas-Pereira, M.B. L. and Nagender Nath, B., 2007b. Native aluminium (spherules and particles) in the Central Indian Basin sediments: Implications on the occurrence of hydrothermal events. *Mar. Geol*., **240**, 177-184.

Iyer, S.D., Prasad, M.S., Gupta, S.M. and Charan, S.N., 1997. Evidence for Hydrothermal activity in the Central Indian Basin. *Deep-Sea Res.,* **44,** 1167-1184.

Izett, G. A., 1981. Volcanic ash beds: recorders of Upper Cenozoic silicic pyroclastic volcanism in the western United States. *Jour. Geophys. Res*., **86**, 10200-10222.

Kastner, M. and Stonecipher, S.A., 1978. Zeolites in pelagic sediments of the Atlantic, Pacific and Indian Oceans. In: Natural zeolites: Occurrences, Properties and Uses (L.B. Sand and F.A. Mumpton, eds.), pp. 199-220. Pergamon Press, Oxford.

Kolla, V., and Biscaye, P.E., 1973. Deep-sea zeolites: Variations in space and time. *Mar. Geol.,* **15,** M11-M17.

Lisitzin, A. P., 1996. Oceanic sedimentation: Lithology and geochemistry (translated by Woolhiser, R. C.), American Geophysical Union, Washington, D.C., USA, 400 pp.

Martin-Barajas, A. and Lallier-Verges, E., 1993. Ash layers and pumice in the Central Indian Basin: Relationship to the formation of manganese nodules. *Mar. Geol.,* **115,** 307-329.

Mascarenhas-Pereira, M.B.L., Nath, B.N., Borole, D.V. and Gupta, S.M., 2006. Nature, source and composition of volcanic ash in sediments from a fracture zone trace of Rodriguez Triple Junction in the Central Indian Basin. *Mar. Geol*., **229**, 79-90.

Mascarenhas-Pereira, M.B. L. and Nagender Nath, B., 2010. Selective leaching studies of sediments from a seamount flank in the Central Indian Basin: Resolving hydrothermal, volcanogenic and terrigenous sources using major, trace and rare-earth elements. *Mar. Chem*., **121**, 49-66.

Mukherjee, A.D. and Iyer, S.D., 1999. Synthesis of morphotectonics and volcanic of the Central Indian Ocean Basin. *Curr. Sci.,* **75,** 296-304.

Mukhopadhyay, S., Dasgupta, S. and Roy, S., 1988. Distribution and characteristics of micronodules in the pelagic sediments from Central Indian Basin, Indian Ocean, and their implications. *Mar. Min.,* **7**, 351-360.

Mukhopadhyay, R., Ghosh, A. K. and Iyer, S. D., 2008. The Indian Ocean nodule field: Geology and resource potential (Handbook Exploration Environ. Geochem. 10; (Hale, M. ed.). Elsevier, Amsterdam, The Netherlands, 292 pp.

Nath, B.N., 2001. Geochemistry of sediments. In: The Indian Ocean: A Perspective (R. SenGupta and E. Desa, eds.), **2**, pp. 645-689. Oxford & IBH, New Delhi, India.

Nath, B.N., Rao, V.P.C. and Becker, K.P., 1989. Geochemical evidence of terrigenous influence in deep-sea sediments upto 8^{o} S in the Central Indian Basin. Mar. Geol., **87**, 301-313.

Nath, B.N., Roelandts, I., Sudhakar, M. and Pluger, W.L., 1992. Rare earth element patterns of the Central Indian Basin sediments related to their lithology. *Geophys. Res. Lett*., **19**, 1197-1200.

Ninkovich, D., Shackelton, J., Abdel-Monem, A. A., Obradovich, J. D. and Izett, G., 1978. K-Ar age of the late Pleistocene eruption of Toba, north Sumatra. *Nature*, **276**, 574-577***.***

Prasad, M.S., 1994. New occurrences of Australasian microtektites in the Central Indian Basin. *Meteoritics*, **29**, 66-99.

Rose, W.I. and Chesner, C.A., 1987. Dispersal of ash in great Toba eruption, 75 ka. *Geology,* **15,** 913-917.

Rose, W.I. and Chesner, C.A., 1990. Worldwide dispersal of ash and gases from earth's largest known eruption: Toba, Sumatra, 75 ka. *Palaeogeography, Palaeoclimatology,* Palaeoecology (Global and Planetary Change Section), **89**, 269-275.

Royer, J.Y., Sclater, J.G., Sandwell, D.T. and Cande, S.C., 1989. A preliminary tectonics fabric chart of the Indian Ocean. *Proc. Indian Acad. Sci.,* **98**, 7-24.

Sudhakar, M., 1989. Ore grade manganese nodules from the central Indian basin: an evaluation. *Mar. Min*., **8**, 201-214.

Sukumaran, N.P., Banerjee, R., Borole, D.V. and Gupta, S.M., 1999. Some aspects of volcanic ash layers in the Central Indian Basin. *Geo-Mar. Lett.,* **18**, 203-208.

Svalnov, V.N., 1981. The effect of island volcanism in the Indian Ocean. *Oceanology, **21,*** 606-612.

Wohletz, K.H., 1983. Mechanisms of hydrovolcanic pyroclast formation: size, shape, and experimental studies. *Jour. Volcanol. Geotherm. Res*., **17**, 31-63.

List of Tables

Table 1: Down-core occurrence of various coarse fraction components in core GC-1.

Table 2: Description and weight of coarse fraction obtained at depth interval of 2 cm in core GC-1. Bio = biotite, Qtz = quartz, Palg = palagonite, int = interpenetrative twin crystals, 2 int = crystals with interpenetrative twin planes, 3 = crystals with interpenetrative twin planes

Table 3: Average composition of coarse fractions analysed by EDS. The number of grains analysed are within brackets.

List of Figures

Figure 1. Occurrence and variation of coarse fraction percentage with core depth. B = biotite, P = phillipsite, R = radiolarians, F = fish tooth, M = manganese micronodules, G = glass shard, Rx = rock fragments, Pu = pumice clasts. The peaks below 80 cm correspond to micronodules.

Figure 2. Biotite grains depicting perfect basal cleavage. The angular to sub-angular shapes suggest minimal transportation of the grains.

Figure 3. (A) Fresh phillipsite crystals with 3 intersecting, (B) 2 intersecting, (C, D) multiple intersecting twin planes. The freshness of the crystals indicates that dissolution effect was nearly absent.

Figure 4. Twinned crystals of phillipsite with multiple intersecting twin planes. The crystals show features of dissolution and overgrowth of FeMn oxides. Image D is a microtektite with several crater-like features and pits formed due to impact.

Figure 5. Radiolarians (A-D) and fish teeth (E, F).

Figure 6. Ferromanganese micronodules of variable sizes and shapes. Image B is the enlarged part of A with a growth of phillipsite crystal.

Figure 7. Transparent glass shards, flat (A), cuspate (B); translucent shards curved (C), blocky (D); Coloured subspherical shard (E), irregular (F).

Figure 8. Iron-rich fragments (A, B) with sharp angular edges suggest minimum transportation. C-E are pumice clasts, F shows growth of a phillipsite crystal and micronodules over a pumice clast.

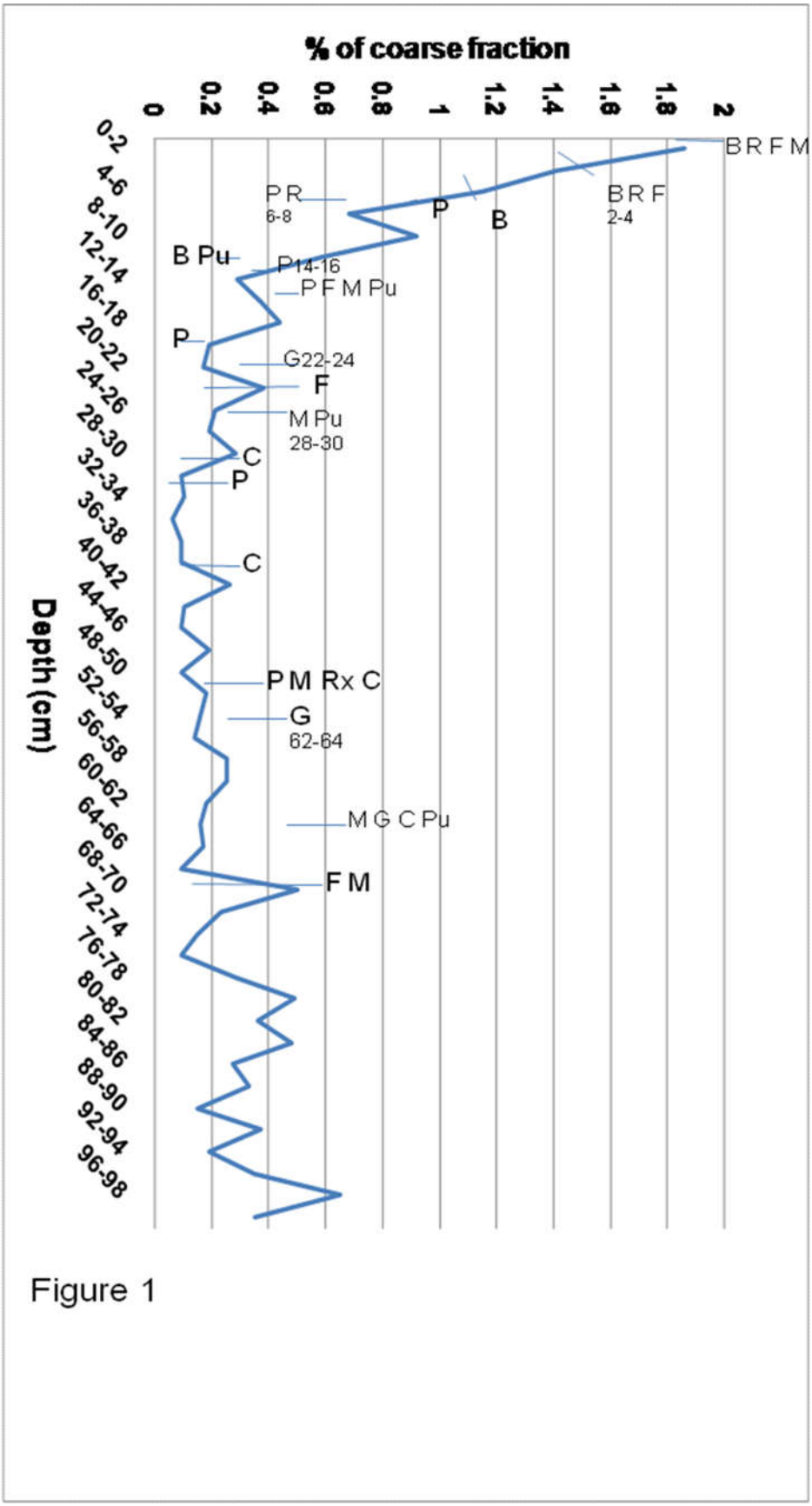
% of coarse fraction
0
0.2
0.4
0.6
0.8
1
1.2
1.4
1.6
1.8
2
Depth (cm)
0-2
4-6
8-10
12-14
16-18
20-22
24-26
28-30
32-34
36-38
40-42
44-46
48-50
52-54
56-58
60-62
64-66
68-70
72-74
76-78
80-82
84-86
88-90
92-94
96-98
B R F M G Rx
P R
6-8
P
B
B R F
2-4
B Pu
P14-16
P F M Pu
P
G22-24
F
M Pu
28-30
C
P
C
P M Rx C
G
62-64
M G C Pu
F M

Figure 1

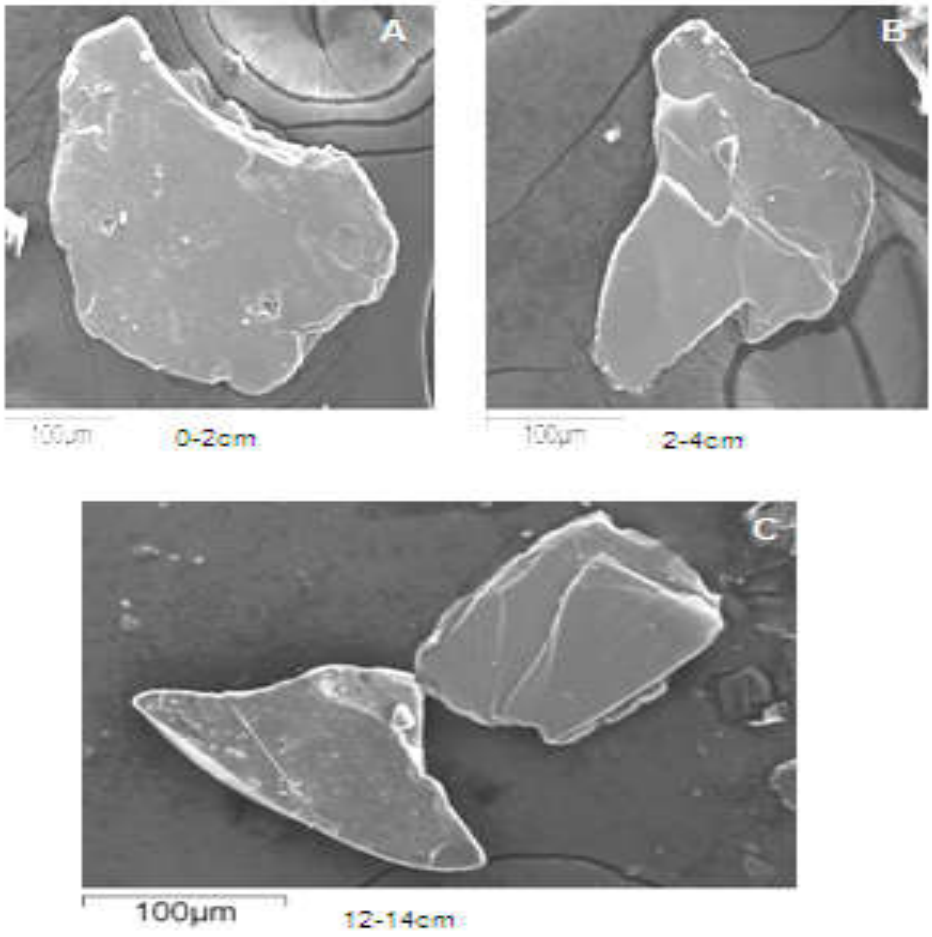

Figure 2

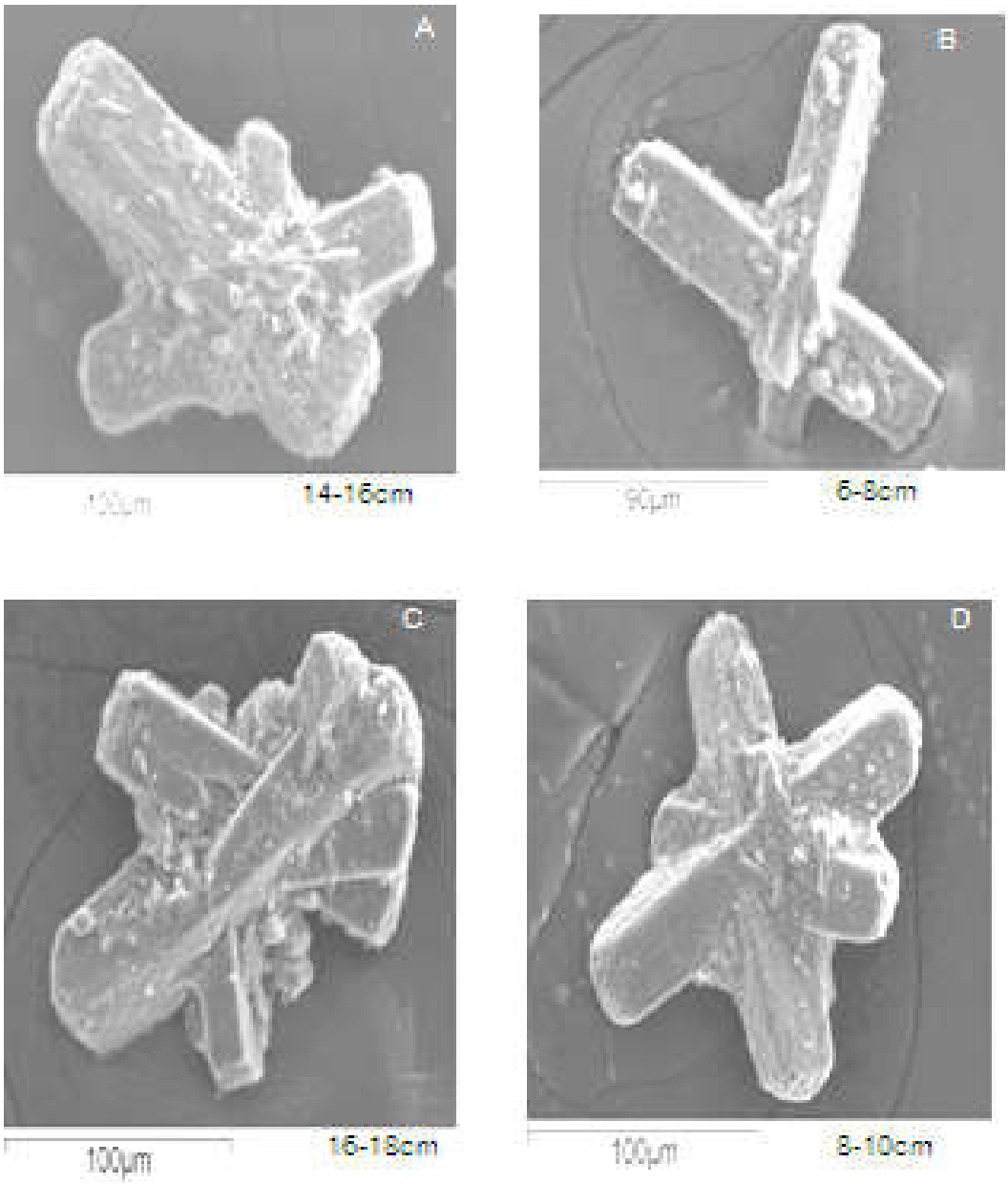

Figure 3

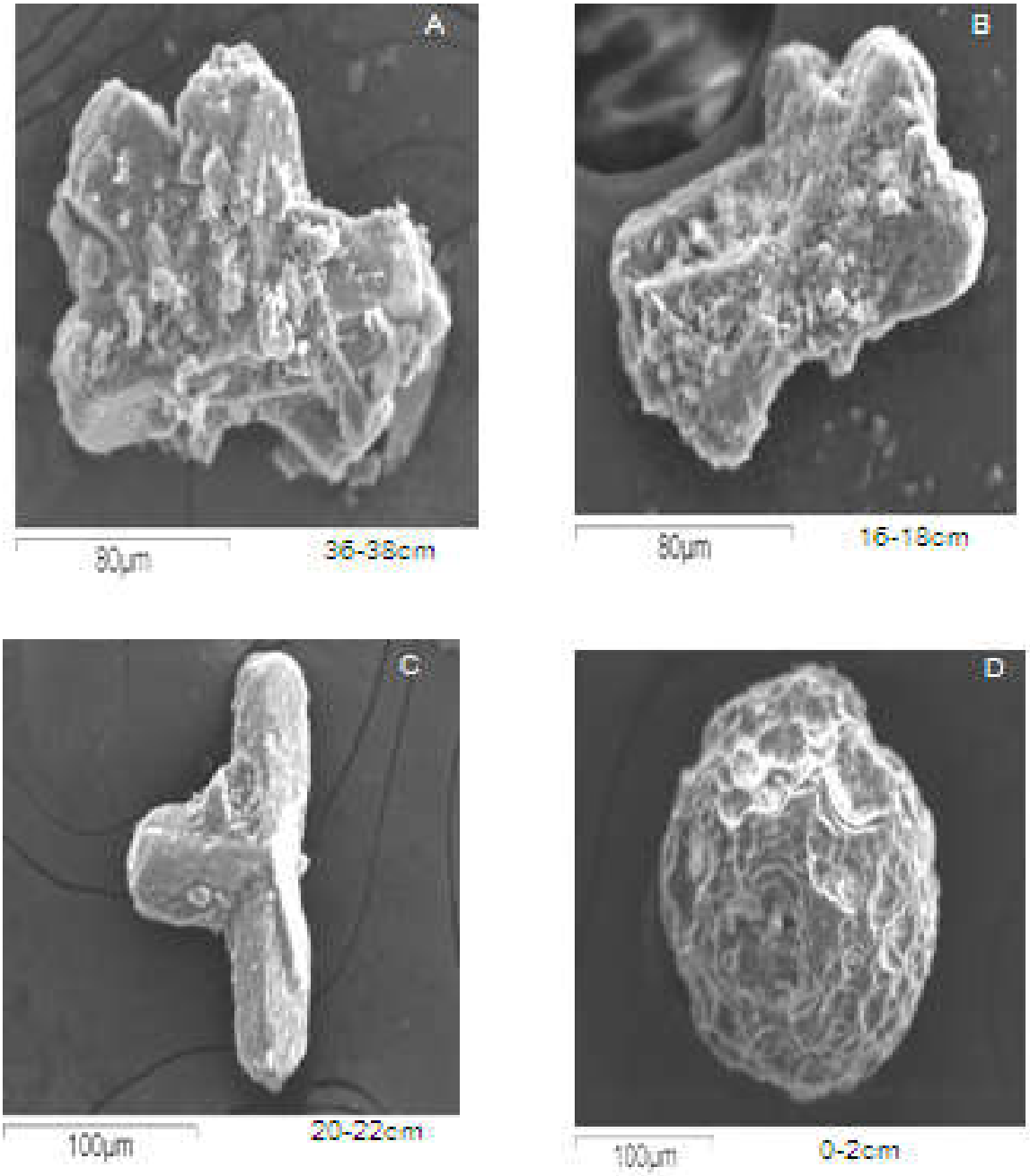

Figure 4

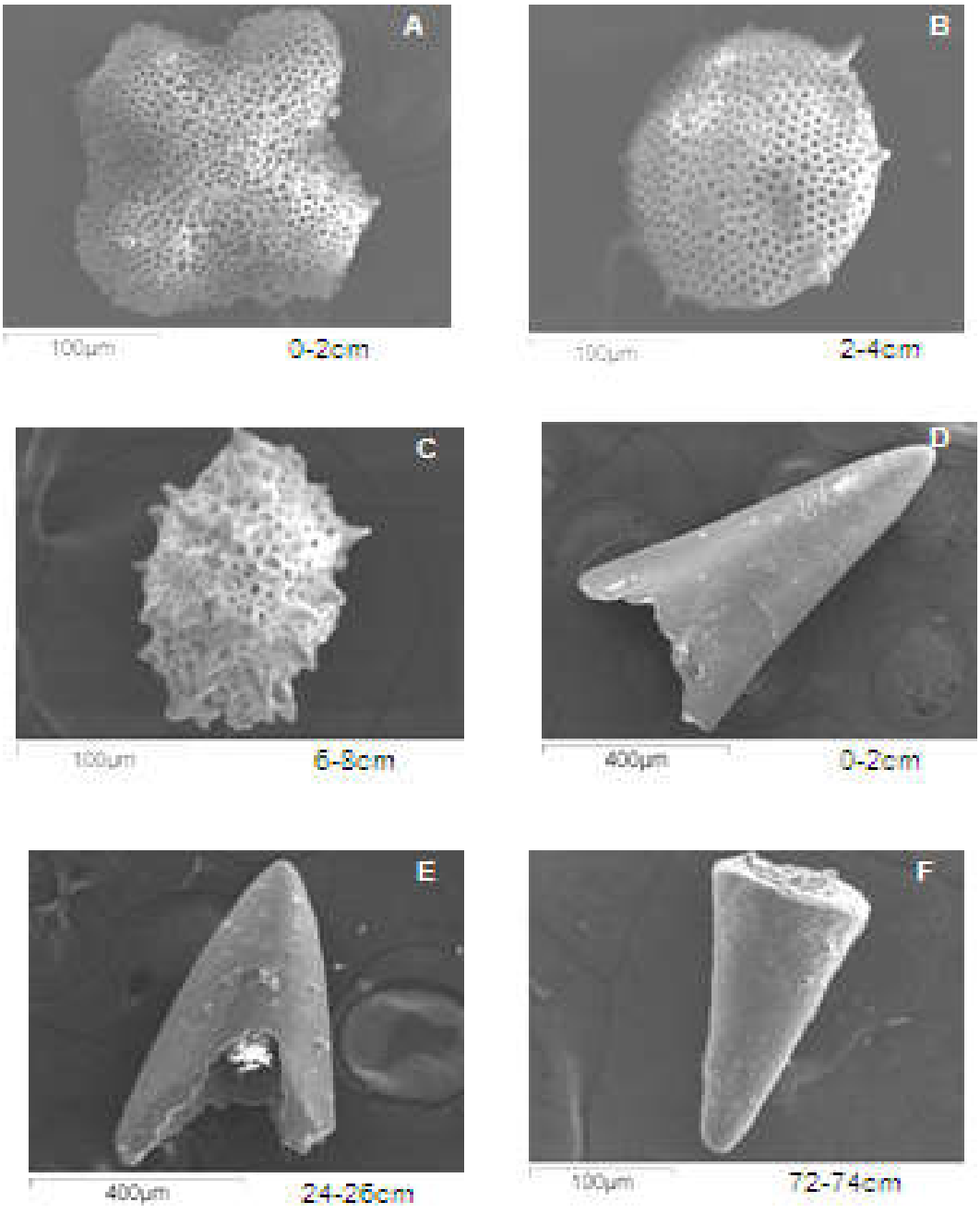
A
100µm
0-2cm
B
100µm
2-4cm
C
100µm
6-8cm
D
400µm
0-2cm
E
400µm
24-26cm
F
100µm
72-74cm

Figure 5

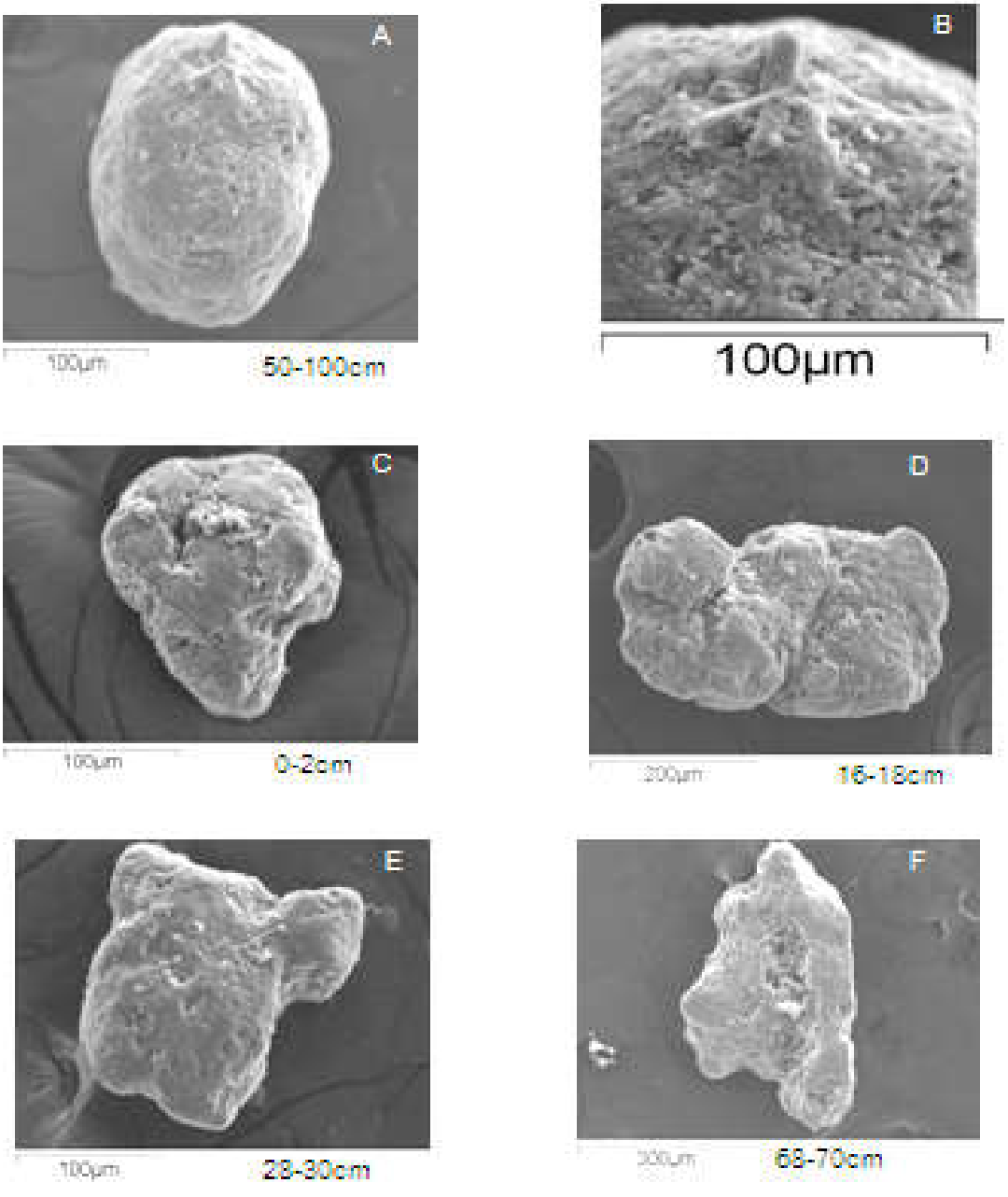
A
100µm
50-100cm
B
100µm
C
100µm
0-2cm
D
16-18cm
E
100µm
28-30cm
F
68-70cm

Figure 6

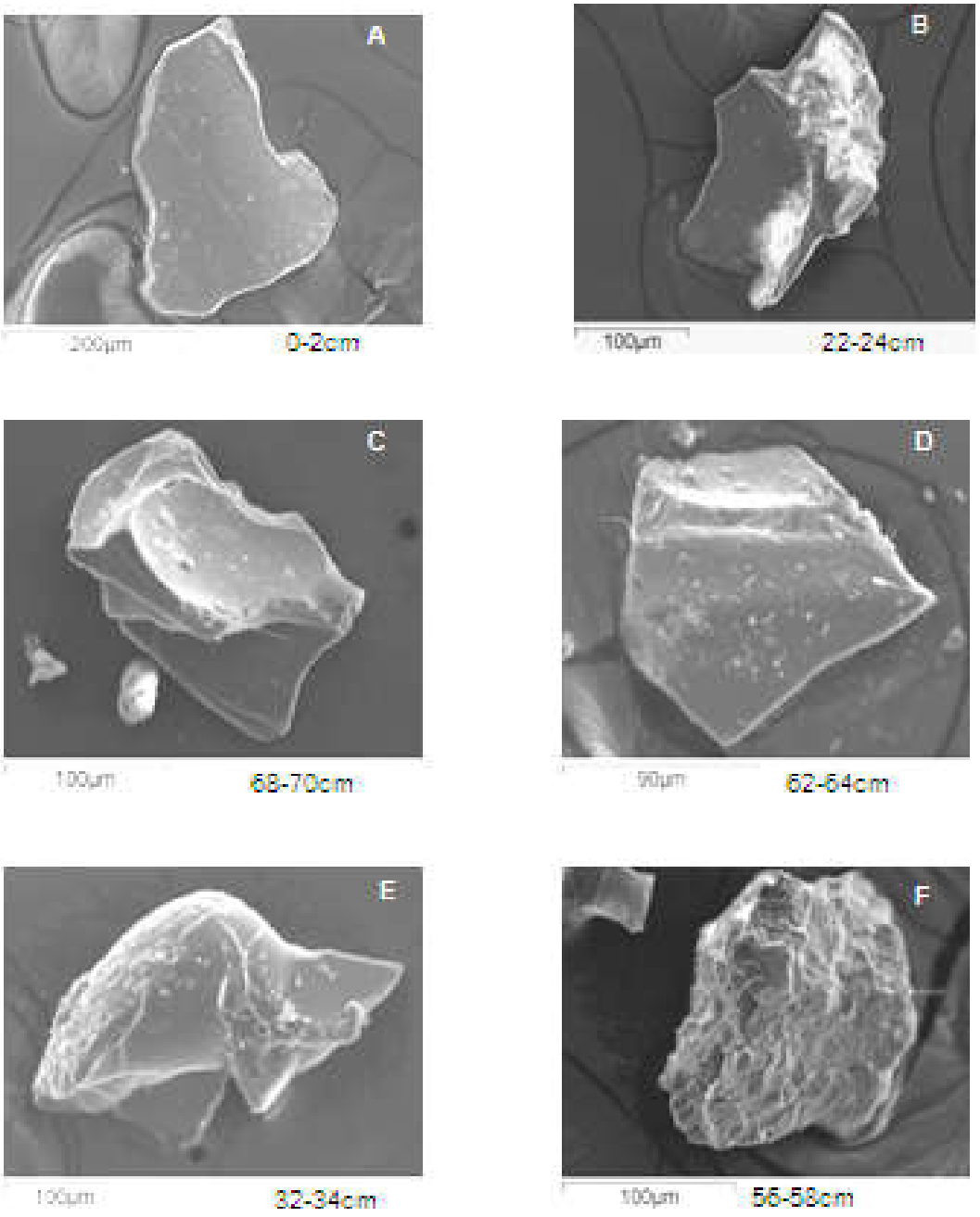
A
200µm
0-2cm
B
100µm
22-24cm
C
100µm
68-70cm
D
90µm
62-64cm
E
100µm
32-34cm
F
100µm
56-58cm

Figure 7

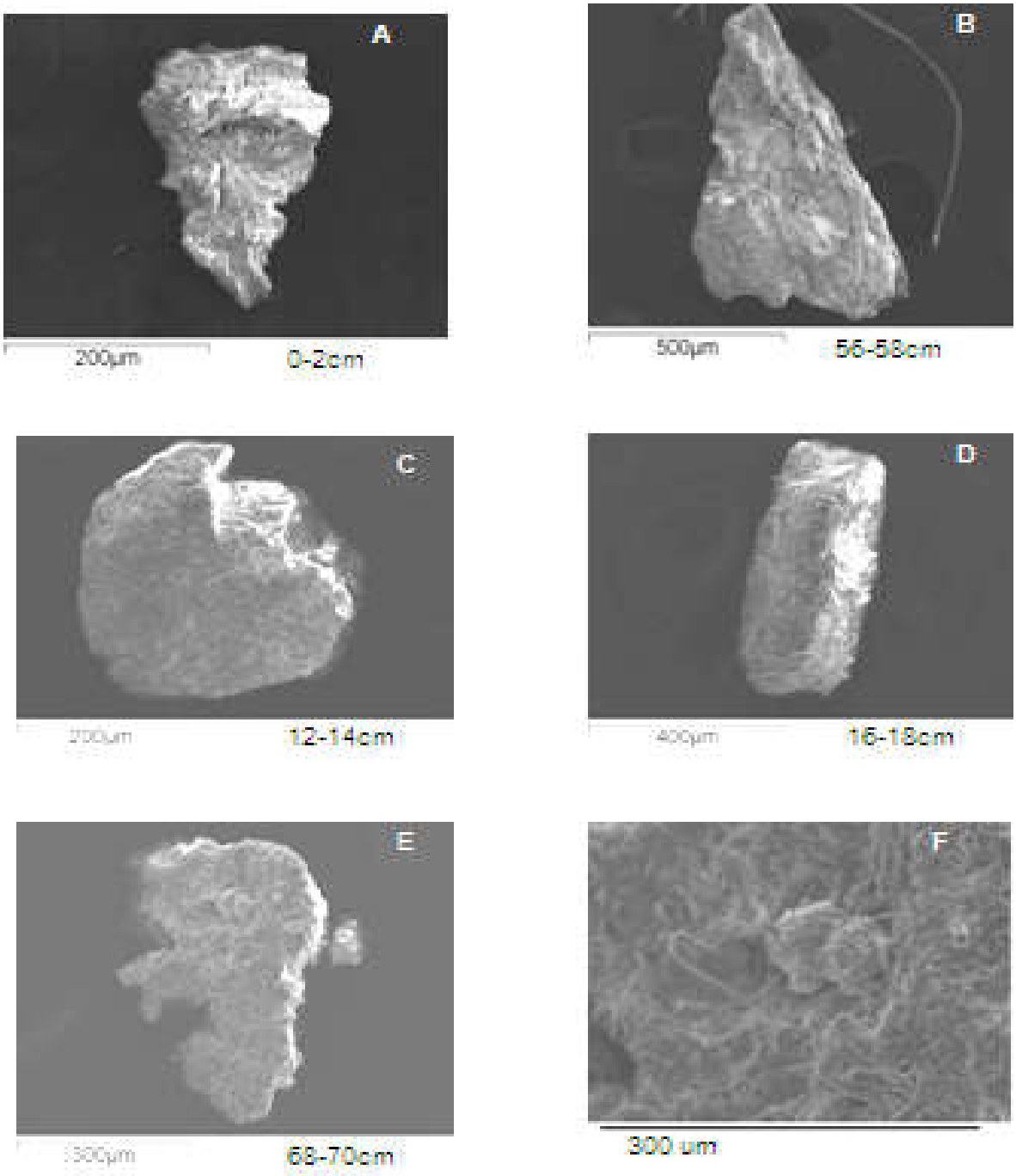

Figure 8

Table 1.

Biotite Flake	Phillipsite crystal	Radio-larian	Fish Tooth	Manganese micronodule	Glass shard	Colour particle	Rock piece	Pumice clast
0-2	14-16	0-2	0-2	0-2	0-2	32-34 red	0-2	12-14
2-4	6-8	2-4	2-4	16-18	0-2	44-46 pink	56-58	16-18
4-6	16-18	6-8	16-18	28-30	0-2	56-58 green	--	28-30
12-14	20-22	0-2	24-26	56-58	22-24	68-70 orange	--	68-70
--	36-38	0-2	72-74	68-70	62-64	--	--	--
--	56-58	0-2	--	72-74	68-70	--	--	--
--	8-10	--	--	50-100	--	--	--	--

Table 2.

Depth (cm)	Coarse fraction (%)	Manganese micro-nodules	Glass shards		Phillips-ite crystals	Pumice clasts	Rock fragment (Basaltic)		Mineral grains	Biogenic matter	Others
			Transparent	Translucent			Fresh	Altered			
0-2	1.86	(36)	Very abundant, platy, bubble, Y-shape	-	2 int (1) 3 int (1)	Plenty	(5)	(4)	Bio (14), Qtz	Fish tooth, Radiolarians spherical star-shape	Micro tektite, fragm-ent of micro tektite, palg (4)
2-4	1.41	(27)	Very abundant, platy, Y-shape bubble, blocky	-	-	Small plenty	pr	(6)	Bio (10) Qtz	-	Fragment of microtektite, palg
4-6	1.15	(2)	Plenty plain	-	-	Small few, Large (2)	-	-	Bio (15)	-	Orange palg (2), red palg (1) Microtektite (1),
6-8	0.68	(19)	Plenty platy, blocky	-	3 int (2)	Plenty large & small	pr	-	Bio (2), Qtz	Radiolarian -spiny-(1)	Microtektite (1)
8-10	0.92	(31)	Plenty platy, blocky	(3)	3 int (1) Multi int (1)	Plenty large & small	-	-	Bio (6)	Radiolarian -spiny-(2)	Fragment of microtektite, green grain

10-12	0.59	(24)	Plenty platy, bubble, blocky	(2)	-	Plenty large & small	-	-	Bio (4), Qtz	-	Microtektite (2)
12-14	0.29	(14)	Plenty platy, blocky	(3), platy	-	Few small	-	-	Bio (3), Qtz	-	Orange palg
14-16	0.37	(31)	Plenty platy	-	3 int (1), Multi int (1)	Large very few, Small many	-	1	Bio (4), Qtz	-	Aggregates palg
16-18	0.44	(68)	Plenty platy, bubble, Y-shape	Elongated (4)	2 int (5) 3 int (1)	Large very abundant, small plenty	(1)	-	Bio (3)	Fish teeth (6), Radiolarian spiny spherical (1)	Aggregates of palg
18-20	0.19	(20)	Abundant, platy, Y-shape	-	2 int (2) 3 int (1)	Plenty, Large few, small many	-	(1)	Bio (2)	Fish tooth (1)	Microtektite-1, Green, orange grains
20-22	0.17	(55)	Plenty platy, Y-shape	-	2 int (4) 3 int (1)	Abundant, large few, small many	-	(1)	-	Fish tooth (1)	White grains pumice-lke (2), palg

22-24	0.38	(62)	Plenty platy, Y-shape	-	2 int (3) 3 int (1)	Abundant, clay filled in vesicle	(1)	-	-	Fish teeth (4)	Brown palg (2)
24-26	0.21	(28)	(28), platy	-	-	Small plenty, Large few	-	-	Bio (1)	Fish teeth (4)	Flaky fragment
26-28	0.19	(30)	(102), platy, Y-shape	-	2 int (3)	Large plenty, small many	(1)	(1)	Bio (1)	-	Red & green grains
28-30	0.28	(35)	(37), platy	(9)	3 int (1)	Plenty, Large (8), Small many	-	-	-	Fish teeth (2)	Red & green grains
30-32	0.09	-	-	-	-	-	-	-	-	-	-
32-34	0.10	(45)	(33), platy, Y-shape	-	2 int (2) 3 int (2)	Large (11), small few	(6)	(2)	Bio (1)	Fish tooth (1)	Greenish white grain, yellow glass
34-36	0.06	(22)	(24), platy	(2), platy	2 int (2)	Large (10), small plenty	-	-	Bio (1)	Fish tooth (1)	Green- white grain

36-38	0.09	(28)	(17), platy,Y-shape	(1) elongate	2 int (2) 3 int (2)	Large (3), Small many	(1)	-	-	Fish tooth (1)	-
38-40	0.09	(97)	(94), platy, Y-shape	(3), platy, elongate	2 int (5)	Large (3), Small many	(1)	-	-	Fish tooth (1)	Microtektite (1), Palg
40-42	0.26	(7)	(7), platy	(1), elongate	-	Large (4), Small many	-	(1)	Bio (1)	-	White flaky fragment
42-44	0.10	(15)	(10), platy, Y-shape	(3), platy	-	Plenty	(2)	-	-	Fish tooth (1)	White grain (1)
44-46	0.09	(31)	(25), platy	(2)	-	Large (3), small many	(1)	-	-	Fish tooth (1)	Aggregate of crystal (1), red palg (2)
46-48	0.19	(70)	Abundant	-	-	-	-	-	-	-	Red, yellow grains
48-50	0.09	(25)	-	-	2 int (2)	-	-	-	-	-	(1) Magnetite spherule
50-52	0.18	(23)	(10), platy	-	-	Large (3), small (19)	(1)	-	-	-	Palg

52-54	0.16	(33)	(18), platy	-	2 int (1) 3 int (1)	Large (4), small many	-	-	Bio (1)	-	Microtektite (1)
54-56	0.14	(46)	(15), platy, blocky	(2), platy	2 int (2)	Plenty, large (5), small many	-	-	-	Fish tooth (1)	Orange & yellow palg
56-58	0.25	(206)	(33), platy, blocky bubble	(10), platy, elongated	2 int (5) 3 int (1)	Abundant	(1)	(3)	Bio (1)	Fish teeth (4)	Red & orange palg, green grain (1)
58-60	0.25	(63)	(24), platy, blocky	(6), platy, elongate	2 int (1)	Plenty	(1)	-	-	Fish tooth (1)	White flaky fragment
60-62	0.18	(43)	(9), platy, blocky	(5), platy	2 int (1)	Large (5), small many	(2)	-	-	Fish tooth (1)	Orange palg
62-64	0.16	(12)	(8), platy, elongate	-	-	(5)	-	-	-	-	White & orange grains
64-66	0.17	(35)	(16), platy, blocky Y-shape	-	3 int (1)	Large (5), small many	(2)	(1)	-	Fish tooth (1)	Orange palg (3)
66-68	0.09	(7)	(3)	-	2 int (1)	(6)	(1)	-	-	-	Aggregates of crystal
68-70	0.50	(171)	(46), platy, blocky Y-shape	(10), platy, elongate	2 int (2) 3 int (1)	Abundant	(2)	(1)	-	-	Green glass (1), White grain
70-72	0.23	(18)	(13), platy, blocky	-	-	Large (4), small (18)	-	-	-	-	Yellow glass (1)
72-74	0.15	(103)	(30), platy, blocky Y-	(3), blocky	2 int (3) 3 int (1)	Large (3), small many	(2)	(1)	-	Fish teeth (3)	Orange, red, yellow, palg,

			shape								
74-76	0.09	(60)	(22), platy, blocky	-	2 int (1)	Large (3), small (13)	-	-	-	-	Orange glass
76-78	0.28	(66)	(10), platy, Y-shape	(1)	-	Large (4), small few	(2)	-	-	-	Orange palg
78-80	0.49	Very few	Few	-	(1)	-	-	-	-	(1) Fish tooth	Coloured grains
80-82	0.36	Very few	Few	-	-	(1)	-	-	-	(1) Fish tooth	-
82-84	0.48	Very few	-	-	-	-	-	-	-	-	coloured glass
84-86	0.27	Few	-	-	-	-	-	-	-	-	(1) green grain
86-88	0.33	(21)	(6), very Small, platy	-	-	Small (7),	-	-	-	-	(1) Microtektite, (1) magnetite spherule
88-90	0.15	(11)	(11), small, spherical	Blocky (2)	-	Small (3)	-	-	-	-	-
90-92	0.37	Very few	-	-	-	-	-	(1)	-	-	-
92-94	0.19	Very few	-	-	-	(1)	-	-	-	-	-
94-96	0.35	Very few	-	-	-	(1)	-	-	-	(1) Fish tooth	-
96-98	0.65	Very few	-	-	-	-	-	-	-	-	-
98-100	0.35	Very few	-	-	-	(1)	(1)	-	-	-	-

Table 3.

Oxide (%)	Biotite (6)	Phillipsite (11)	FeMn micronodules (7)	Glass shards (7)	Pumices (4)	Magnetite spherules (2)	Microtektite (1)
SiO_2	37.65	65.18	19.37	78.92	58.22	5.6	65.22
Al_2O_3	12.80	18.18	6.31	11.35	16.45	1.58	13.41
TiO_2	4.58	0.64	0.61	-	1.00	-	1.06
FeO	26.07	2.49	6.51	1.03	10.17	90.49	8.23
MgO	9.39	1.68	5.85	0.34	3.10	1.57	4.47
CaO	-	1.54	3.72	0.86	3.02	0.95	4.99
Na_2O	0.45	4.02	1.23	2.43	1.16	-	0.57
K_2O	9.28	5.80	1.87	5.35	3.5	-	1.65
NiO	-	-	4.37	-	-	-	-
CuO	-	-	1.32	-	-	-	-
MnO	0.43	-	48.79	-	3.37	0.59	-
Cr_2O_3	-	-	-	-	-	-	0.40